IIETA International Information and Engineering Technology Association
Advancing the World of Information and Engineering

Journal Européen des Systèmes Automatisés
Vol. 55, No. 1, February, 2022, pp. 25-34
Journal homepage: http://iieta.org/journals/jesa

Model Predictive Control for Three-Phase Three-Level NPC Inverter Based APF Interfacing Single Stage Photovoltaic System to the Grid

Abdelkader Lakhdari*, Boualam Benlahbib, Thameur Abdelkrim

Unité de Recherche Appliquée en Energies Renouvelables, URAER, Centre de Développement des Energies Renouvelables, CDER, Ghardaïa 47133, Algeria

Corresponding Author Email: lakhdari_abdelkader@hotmail.com

https://doi.org/10.18280/jesa.550103

Received: 9 December 2021
Accepted: 19 February 2022

Keywords:
TTLNPC inverter, APF, MPPT, model predictive control, cost function

ABSTRACT

A finite control set model predictive control (FCS-MPC) based controller has a fast dynamic response and robustness. furthermore, the presence of a cost function gives designers a degree of freedom to include system control targets, constraints and system non-linearities. On the other hand, Multilevel inverter (MI) topologies are becoming a strong alternative in distributed power generation system (DPGS), among these topologies is the three-phase three-level NPC (TTLNPC) inverter. Generally, to properly operate this topology, the applied current control ensures the achievement of two main objectives. First, the output current must be controlled to track its reference. Second, the two dc-link capacitor voltages have to be equal and balanced. In this paper, FCS-MPC is proposed to control the TTLNPC inverter based parallel active power filter (APF) adopted to connect a photovoltaic system (PVS) to the grid and perform a harmonic mitigation. The proposed FCS-MPC exploit the model of the system to predict the future values of the inverter currents by selecting the best voltage vector that aims to minimize a predefined cost function. Instead of using the popular redundant vectors algorithms to balance the two-split dc-link capacitor voltages, another term will be added to the expression of the cost function to achieve this goal. The PV panel is coupled directly to the inverter without DC/DC converter, the P&O MPPT algorithm is responsible to generate the capacitor reference voltage whatever the climatic conditions are. Simulations using Matlab/Simulink were performed to prove the efficiency of the proposed technique to mitigate the grid current harmonics, and to ensure a continuous power injection and perform a load power sharing.

1. INTRODUCTION

PVSs are becoming increasingly applied in the distribution network; they can be grouped as two main categories, Grid tied and standalone systems [1-4]. Grid-tied PV systems (GTPSs) are cost-effective because they do not require storage systems which implies to a reduced investment cost [4]. Single and two-stage systems are commonly used topologies in a GTPS [5, 6]. Two-stage system has certain drawbacks: less efficiency, being larger and more expensive. Therefore, single-stage topology characterized by small size, lower cost, higher efficiency and reliability seems to be more attractive than a system with two stages.

In a GTPS, the algorithm used to extract the maximum available solar power, the conversion efficiency and quality of the total power fed into the grid, are the main criteria employed to judge the performance of the system. These performance criteria are strongly relevant to the topology and the technique used to control the DC/AC power stage. Several topologies of inverters that can be used have been reported in the literature [7], one of the most promising topologies is the multilevel inverters (MIs); the main benefits of this topology are the stepped output voltage waveform due to the higher output voltage levels, it looks like a sinusoid more closely than the traditional inverters [8]. This advantage has prompted researchers to use MIs in GTPS applications, especially in single stage systems as the PV panels are directly connected to the dc-link voltage. Furthermore, in MIs, even though a greater number of power semiconductor devices are involved, but each device switches only for a portion of one fundamental period and therefore, individual device switching frequency (SWF) is reduced [9].

However, the most used MIs are mainly limited to three-level (3L) inverters. If we increase the number of levels, we increase also the degree of control complexity in the goal to keep balanced and equal the two dc-link capacitor voltages meanwhile controlling the complex switching operation of APF [10, 11].

On the other hand, the advanced technologies used in the fabrication of power electronic switches-based semiconductors (IGBTs, MOSFETs, etc.) composing the power converters, as well non-linear loads (NLL) (such as the diode rectifiers) are known to cause a harmful effect (harmonics, decreasing the power factor, etc.) on electric power systems. They consume harmonic currents cause the distortion of the grid current waveforms, implying an increase in their THD. The active filters introduce compensating currents into the source to mitigate the current harmonics and compensate the reactive power drawn by a NLL. Since the potential of active filtering task does not need changes to the power stage. Also, in order to increase the efficiency of PVSs; single-or three-phase 3L-MIs are becoming a strong

alternative to interface PVSs to the power grid [4, 12, 13]. Therefore, a single stage PVS combined with an active filter can be more convenient for the application in the DPGS.

Control of APF is very crucial stage as it decides the overall performance of the APF. Many techniques have been reported in the literature; most of them are dedicated to the most popular three-phase two-level (2L) inverter, hysteresis current control [14], the instantaneous p-q theory [15], synchronous reference frame (SRF) or d-q theory [16, 17], and direct power control (DPC) [18-20]. Their simple principle and easy implementation make them widely used to enhance the power quality, but they still have some drawbacks such as poor dynamic response and their bandwidth limitation which weaken the compensation quality [21, 22].

Recently, FCS-MPC has been widely adopted for power converters control, thanks to the numerous advantages that it can provide: in dynamic (fast dynamic response) as well in steady state (stability and precision) response. Furthermore, it gives the possibility to include the system nonlinearities and constraints in the controller [23, 24]. The FCS-MPC is used to control the three-phase 2L inverter based APF [25], at the same time interface a two-stage PVS to the power grid. Where the used cost function minimizes the error between the reference and predicted values of the APF currents. The FCS-MPC is used to control the three-phase 2L inverter based APF indirectly to interface a wind system to the grid [22], this means that the grid currents were the control currents. In the goal to exploit the performance of multilevel topology and the FCS-MPC technique, this work proposes a TTLNPC inverter based APF is adopted to mitigate the grid current distortion and compensate the reactive power drawn by the NLL, at the same time inject the active power extracted from a single stage PVS to the grid, and share with it the load requirements.

2. PROPOSED SYSTEM CONFIGURATION

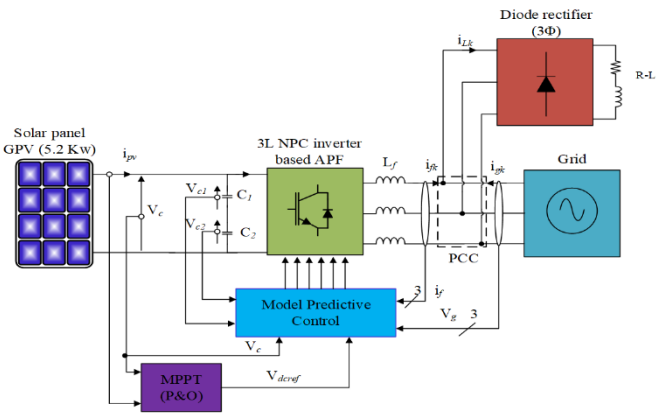

Figure 1. Proposed PVS connected through a TTLNPC inverter based APF

As illustrated in Figure 1, The PVS is coupled to the TTLNPC inverter based APF via a dc-link capacitor. The PV generator (GPV) is coupled directly to the inverter without DC/DC converter, the MPPT gives at each cycle the updated value of the capacitor reference voltage V_{cref} whatever the climatic conditions are. This power is fed to the grid by the means of the APF, the inductor L_f at the output of the APF play the role to reduce the current harmonics and transform the APF from voltage to current source. At the point of common coupling (PCC) and in parallel with the APF and the utility grid, a NLL (diode rectifier feeds a resistor in series with an inductor) is connected. At full sunny-days, only the PVS takes the role to supply the load power requirements, any extra amount of power will be fed directly to the grid.

At full or partially cloudy-days, and if the power drawn from the PVS is not capable to feed the load needs, the power network will share the PVS by providing the deficit of power to reach the load power requirements. While the operation of the system, the APF takes the role to inject the power generated by the PVS to the PCC and performs reactive power compensation and mitigates the grid current harmonics.

In this work, a PV panel of 5.2 kW composed by the connection in series (Ns = 17) and parallel (Np = 4) of PV modules of 76 W (composed by coupling 36 PV cells in series) is used.

3. MPPT ALGORITHM

As known, the GPV has a non-linear P-V characteristics presenting one maximum power point (MPP) located by two coordinates (In our case: Impp = 4.52 A, Vmpp= 16.84 V). Extracting maximum power is one step essential in a photovoltaic conversion system. An MPP tracking algorithm (MPPT) is applied to the DC / DC converter in the case of a two-power stage and to the DC / AC converter in the case of a single power stage. In this article, the maximization algorithm P&O is used, adopted for its simplicity and ease implementation. As the name suggests, its principle is simple, disturb the output power of the solar panel by disturbing (increment or decrement) its voltage in one direction, then observe the panel output power if it has been increased or decreased. The direction which leads to increase the output power will be kept for the next disturbance as shown in the flowchart of Figure 2.

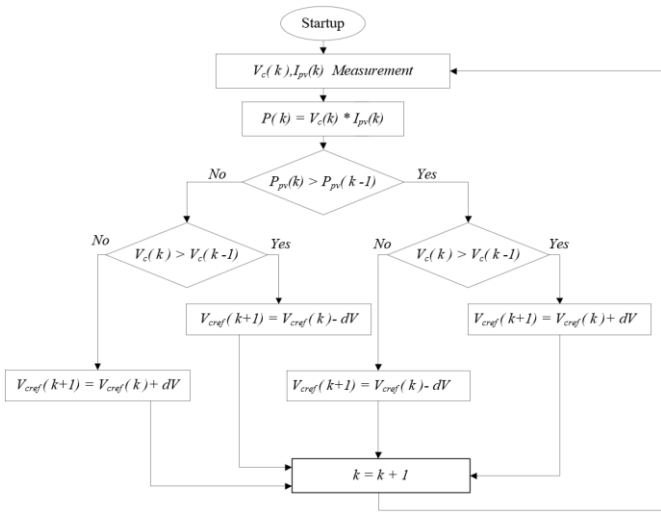

Figure 2. P&O algorithm flowchart

where:

$V_c(k)$: Actual value of PV panel voltage (APF dc-link input).

$V_c(k-1)$: Previous value of the PV panel voltage.

$I_{pv}(k)$: Actual value of PV panel current.

$P_{pv}(k)$: Actual value of PV panel power.

$P_{pv}(k-1)$: Previous value of the PV panel power.

dV: Output voltage perturbation.

V_{cref}: Updated value used to track the PV panel optimal voltage.

4. THREE-PHASE TTLNPC INVERTER BASED APF CONTROL

The FCS-MPC applied to the TTLNPC inverter based APF is articulated on the prediction of the future behavior of the filter compensating currents using the model of the whole system (Grid + APF + NLL). Based on this information, the controller will choose among the large 27 possible APF voltage vectors the optimal voltage vector that aims to minimize a prior defined function selected in accordance with control requirements.

At each sampling time Ts, The FCS-MPC controller evaluates all 27 vectors to calculate the corresponding (k+1) predicted value of the APF current. The vector (switching state (SS)) which gives a lower cost function value will be selected and sent to APF switches in the next sampling time.

Since the TTLNPC inverter has a number of switches higher than its counterpart of 2L inverter has, presenting 27 SSs producing 19 different voltage vectors. high number of possible vectors means additional degrees of freedom and various possibilities for the choice of the cost function to be envisaged [26].

Figure 3 shows the power circuit of a TTLNPC inverter [26], four switches and two diodes are composing each leg of the inverter. By the mean of these diodes and the medium switches, the output terminals can be connected to the neutral point of the dc-link. So, three voltage levels can be found with respect to the neutral point 0 as shown in Table 1. It can be noted that only two switches conduct at any time. Where Sx refer to the SS of one phase with x = {k, l, m}. More details about the TTLNPC inverter and its possible voltage vectors in the refs. [26, 27].

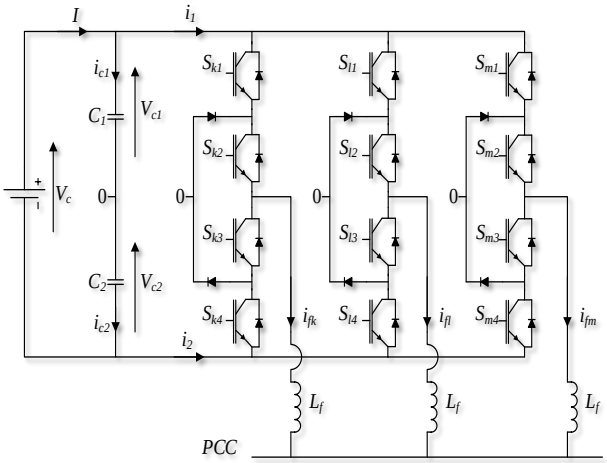

Figure 3. TTLNPC inverter power circuit

Table 1. SSs for one leg of TTLNPC

S_{xj}	S_{x1}	S_{x2}	S_{x3}	S_{x4}	V_{x0}
+	1	1	0	0	$+Vc/2$
0	0	1	1	0	0
-	0	0	1	1	$-Vc/2$

This FCS-MPC technique applied to the TTLNPC inverter used as an APF is summarized in the following steps [25, 26, 28]:

- Specify a desired cost function Cf.
- Establish the TTLNPC inverter model and all 27 possible voltage vectors.
- Establish the TTLNPC inverter based APF model (coupled to NLL and grid) to extract the filter current prediction law.

For the TTLNPC inverter used as an APF, the FCS-MPC must force the APF to compensate the harmonic currents and supply the reactive power needed to feed the connected NLL and keep the sinusoidal form of the grid currents, to achieve this function and for a proper operation of the APF, the two capacitor voltages have to be balanced and controlled. If this balance not achieved, the two dc-link voltages will deviate causing a considerable effect on the output voltage and reduce the performance of the filtering function. Hence the appropriate cost function to be used is that minimizes the error between the predicted and reference values of the APF currents and minimizes also the error between the two-split dc-link voltages in order to keep them constant and balanced as written in Eq. (1):

$$\begin{aligned} Cf = & \left|i^*_{f\alpha}(k+1) - i^p_{f\alpha}(k+1)\right| + \left|i^*_{f\beta}(k+1) - i^p_{f\beta}(k+1)\right| + \\ & + \lambda_c * \left|V^p_{c1}(k+1) - V^p_{c2}(k+1)\right| + \\ & + \lambda_{sw} * \left(\sum_{j=1,2} \sum_{x=k,l,m} \left| S_{xj}(k) - S_{xj,opt}(k) \right| \right) \end{aligned} \quad (1)$$

where, $i^p_{f\alpha}(k+1)$, $i^*_{f\alpha}(k+1)$ and $i^p_{f_\beta}(k+1)$, $i^*_{f_\beta}(k+1)$ indicate the real and imaginary parts of the predicted and reference APF currents in the $\alpha\beta$ coordinates respectively, $V^p_{c1}(k+1)$ and $V^p_{c2}(k+1)$ indicate the predicted values of the dc-link capacitor voltages, λ_c and λ_{sw} are the weighting factors used in the dc-link capacitor voltages balancing, and reduce the TTNPC inverter based APF switching frequency respectively. All quantities are performed in $\alpha\beta$ coordinates and not in dq coordintates frame just to reduce the online calculation burden incurred in one sampling instant.

But, the APF reference current in the next sampling time $i^*_f(k+1)$ is unknown; hence, a second order extrapolation can be used as shown in Eq. (2):

$$i^*_f(k+1) = 3i^*_f(k) - 3i^*_f(k-1) + i^*_f(k-2) \quad (2)$$

For a small sampling time; we can assume that $i^*_f(k+1) = i^*_f(k)$ and no any extrapolation is needed [21].

The proposed predictive current control is implemented by following these steps:

- The APF compensating current $i_f(k)$ is obtained from current sensors and converted to $\alpha\beta$ coordinates. The dc-link voltage control loop acts on the amplitude of grid current which will be used to generate the APF reference current.
- The extracted prediction law will be used to calculate for each vector of the 27 possible voltage vectors the corresponding $(k+1)$ predicted value of the APF compensating current $i^p_f(k+1)$.
- The cost function Cf evaluates the error (to be minimized) between each value of 27 predicted values of filter current (calculated above) and the generated reference current, and minimizes also the error between

the predicted dc-link capacitor voltages $V_{c1}^{p}(k+1)$ and $V_{c2}^{p}(k+1)$ with minimum possible commutations.

- The voltage vector which succeeds to minimize the cost function will be elected as optimal vector and applied to control the APF.

4.1 TTLNPC inverter based APF model

The equivalent circuit of an APF coupled in parallel with NLL and grid is shown in the Figure 4 [18, 22, 25]. From the Figure 4, applying Kirchhoff's voltage law, we can write:

$$V_g - V_{PCC} = R_g * i_g + L_g \frac{di_g}{dt} \tag{3}$$

$$V_f - V_{PCC} = R_f * i_f + L_f \frac{di_f}{dt} \tag{4}$$

The grid and filter resistances R_g and R_f are very small, hence they can be neglected. By subtracting Eq. (4) from Eq. (3) we find:

$$V_g - V_f = L_g \frac{di_g}{dt} - L_f \frac{di_f}{dt} \tag{5}$$

The NLL current has two components, fundamental component $i_{L,f}$ and harmonic component $i_{L,h}$:

$$i_L = i_{L,h} + i_{L,f} \tag{6}$$

On the other hand:

$$i_L = i_f + i_g \tag{7}$$

From Eq. (7) and Eq. (8), we obtain:

$$i_{L,h} + i_{L,f} = i_f + i_g \tag{8}$$

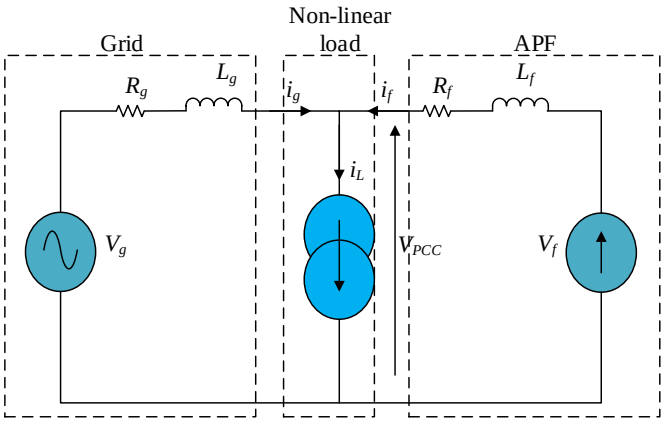

Figure 4. Equivalent circuit of an APF coupled in parallel with NLL and grid

Hence, we can write:

$$i_{L,h} - i_f = -\left(i_{L,f} - i_g\right) \Rightarrow \Delta i_f = -\Delta i_g \tag{9}$$

For a small current variation, we can consider $\Delta i \approx di$, Eq. (9) become:

$$di_g = -di_f \tag{10}$$

By substituting Eq. (10) in Eq. (5), the final electrical equation can be given as:

$$V_f - V_g = L_T \frac{di_f}{dt} / \quad L_T = \left(L_g + L_f\right) \tag{11}$$

4.2 TTLNPC inverter discrete time model

In FCS-MPC, the discrete time model is indispensable to extract the prediction law of the filter current $i_f^p(k+1)$ using the actual measurements $i_f(k)$, $V_g(k)$ and $V_f(k)$. The derivative $\frac{di_f}{dt}$ can be estimated using a simple forward Euler approximation:

$$\frac{di_f}{dt} \approx \frac{\Delta i_f}{\Delta t} = \frac{i_f(k+1) - i_f(k)}{T_s} \tag{12}$$

By substituting the Eq. (12) in Eq. (11), the prediction law gives the APF compensating current is:

$$i_f^p(k+1) = i_f(k) + \frac{T_s}{L_T} * \left(V_f(k) - V_g(k)\right) \tag{13}$$

The differential equations describing the dynamics of the dc-link capacitor voltages are:

$$\frac{dV_{c1}}{dt} = \frac{1}{C_1} i_{c1} \tag{14}$$

$$\frac{dV_{c2}}{dt} = \frac{1}{C_2} i_{c2} \tag{15}$$

where, C_1 and C_2 are the capacitor values of the two dc-link V_{c1} and V_{c2} respectively.

Applying the same approximation for the derivative considered in Eq. (12):

$$\frac{dV_{cx}}{dt} \approx \frac{\Delta V_{cx}}{\Delta t} = \frac{V_{cx}(k+1) - V_{cx}(k)}{T_s} \tag{16}$$

The discrete time equations giving the predicted values of $V_{c1}^{p}(k+1)$ and $V_{c2}^{p}(k+1)$ are:

$$V_{c1}^{p}(k+1) = V_{c1}(k) + \frac{1}{C_1} * i_{c1}(k) * T_s \tag{17}$$

$$V_{c2}^{p}(k+1) = V_{c2}(k) + \frac{1}{C2} * i_{c2}(k) * T_s \tag{18}$$

The currents i_{c1} and i_{c2} depend on the input current and the SSs of the inverter as expressed in Eq. (19) and Eq. (20):

$$i_{c1}(k) = I(k) - G_{1k} * i_{fk}(k) - G_{1l} * i_{fl}(k) - G_{1m} * i_{fm}(k) \quad (19)$$

$$i_{c2}(k) = I(k) + G_{2k} * i_{fk}(k) + G_{2l} * i_{fl}(k) + G_{2m} * i_{fm}(k) \quad (20)$$

where, I is the current at the input of the dc-link capacitor voltages, and G_{1x}, G_{2x} are variables function of the switches states S_x as following:

$$G_{1x} = \begin{cases} 1 & if\ S_x = "+" \\ 0 & otherwise \end{cases} \quad (21)$$

$$G_{2x} = \begin{cases} 1 & if\ S_x = "-" \\ 0 & otherwise \end{cases} \quad (22)$$

with $x = k, l, m.$

4.3 DC-bus control and APF reference current generation

The dc-link control is essential to generate the APF reference current. First, a PI regulator is responsible to maintain the input capacitor voltage V_c constant around its reference value V_{cref} generated by the MPPT block when the PVS is operational. If any dysfunction happens to the PVS for any reason, the PVS will be disconnected from the grid, and the reference value V_{cref} will not be generated by the MPPT block. Hence, a fixed value ($V_{cref} = 300\ V$) will be set. The Figure 5 illustrates the functional scheme of the dc-link regulation.

In Figure 6, the technique used to generate the APF reference current is presented. The dc-link control loop gives the maximum amplitude (I_{gmax}) of the grid reference current. With the help of a PLL block (used to extract the grid voltage angle to synchronize the generated reference current with the grid voltage), the grid reference currents (i_{gk}^*, i_{gl}^*, i_{gm}^*) can be estimated, then subtracted from the load currents to estimate the APF reference currents (i_{fk}^*, i_{fl}^*, i_{fm}^*).

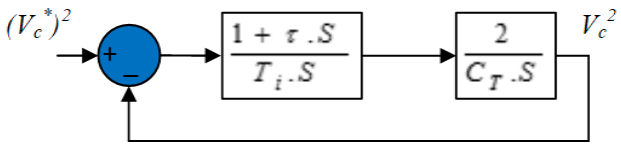

Figure 5. Dc-link voltage control loop

where, $C_T = \dfrac{C_1 . C_2}{C_1 + C_2}$.

Figure 7 shows the flowchart of the FCS-MPC used to control the APF.

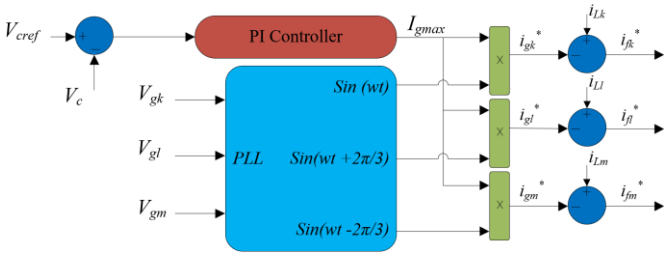

Figure 6. Reference current generation block diagram

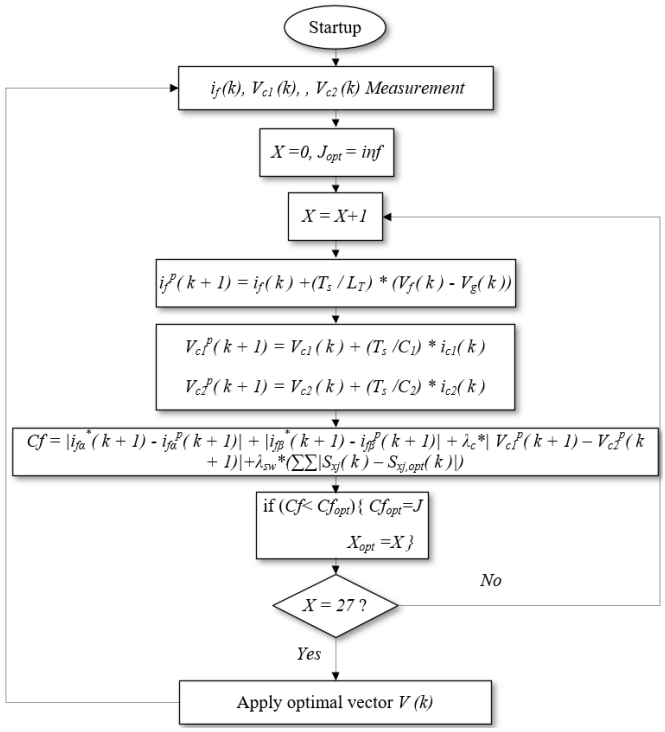

Figure 7. Flowchart of the proposed FSC-MPC applied to the three phase NPC inverter

5. SIMULATION AND DISCUSSION

Simulations have been performed using MATLAB/SIMULINK to evaluate and demonstrate the performance of the proposed PVS and the FCS-MPC used for the TTLNPC inverter based APF using the following operating conditions:

Grid: $V_{grms} = 50V$, $f_g = 50Hz$, $R_g = 0.1\Omega$, $L_g = 0.1mH$.

APF: $L_f = 2mH$, $C_1 = C_2 = 5500\mu f$, $\lambda_c = 0.5$, $\lambda_{sw} = 0$ sampling time: $T_s = 1e - 5$.

Firstly, in the absence of the APF, the load is directly fed by the grid, the load required power (active and reactive power) is supplied by the grid, which means that (Pload = Pgrid & Qload = Qgrid, where P and Q indicate the active and reactive power respectively).

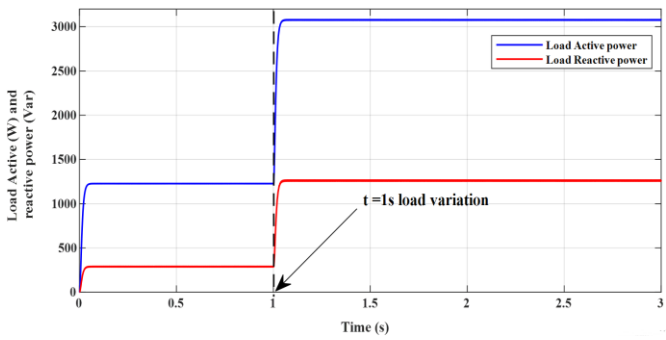

Figure 8. Non-linear load's active and reactive power profile

Figures 8 and 9 show the load consumed active and reactive power, the deformation and the corresponding harmonic contenent of the grid current (load current, phase a) produced by the NLL respectively, the active and reactive power drawn by the connected NLL are respectively PL1 ≈ 1.2 kW and QL1 ≈ 300 Var, at t = 1s a change in the load profile is introduced;

the active and reactive power drawn by the new load are respectively PL2 ≈ 3.1 kW and QL2 ≈ 1.3 kVar. It can be seen from these figures that the NLL (diode rectifier connected to a series R-L load) deform ate the sinusoidal shape of the grid current which is well proven by the h harmonic contenent (THDi = 23.65%) as illustrated in the Figure 9.

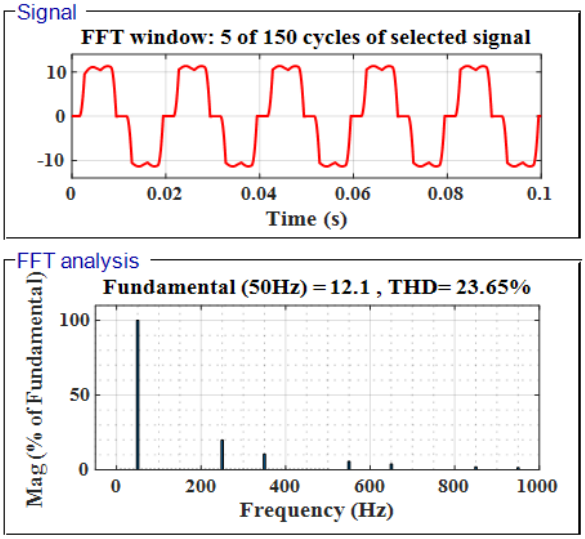

Figure 9. Distortion and harmonic contenent of the grid current

After that, we re-run the system with the insertion of the PVS connected through TTLNPC inverter based APF. The whole system has been tested under two operation modes: (PVS + APF) mode and APF mode only when a dysfunction occurs to the PVS for any reasons.

5.1 Mode of operation 1 (PVS + APF)

In this mode, the power extracted from the PVS will be injected directly to the PCC via the TTLNPC inverter based APF, the grid and the TTLNPC inverter based APF work in conjunction to feed the NLL requirements. The profile of the applied irradiance and the corresponding maximum power extracted from the GPV are shown in Figure 10, these results show the effectiveness of the P&O algorithm in dynamic and steady states to generate the proper value of the reference voltage V_{cref} at any moment whatever the climatic conditions are.

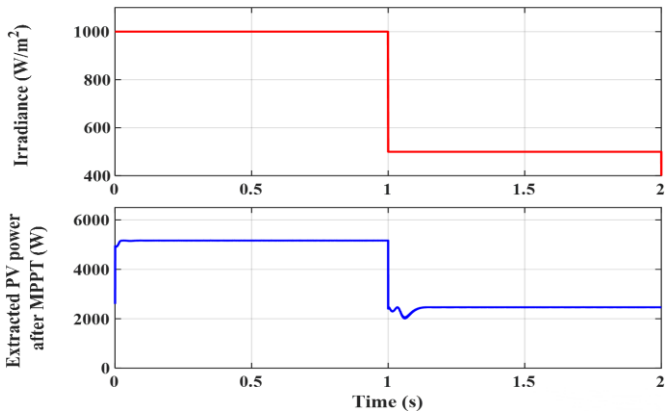

Figure 10. Irradiance profile and the corresponding extracted PV power

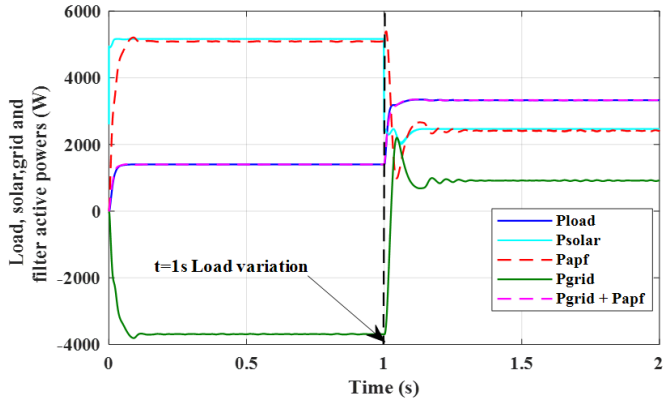

Figure 11. Load active power sharing between the grid and the TTLNPC inverter based APF

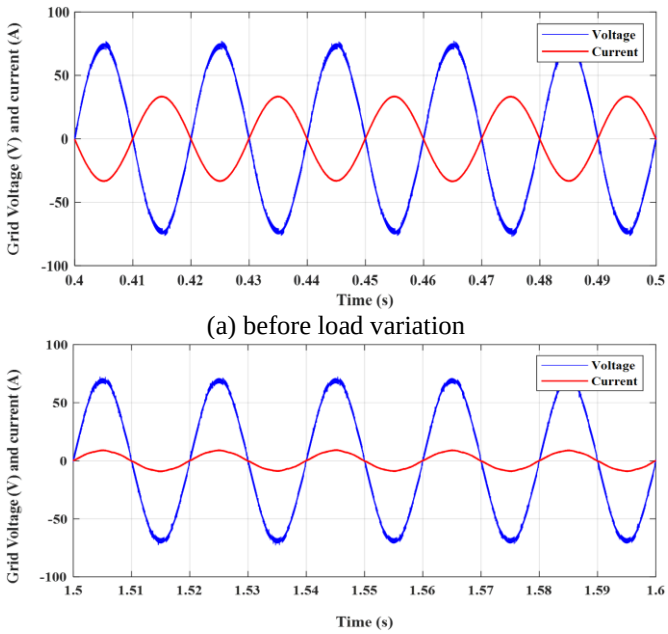

(a) before load variation

(b) after load variation

Figure 12. Grid voltage and current

Figures 11 and 12 shows the contribution of the TTLNPC inverter based APF to fulfill the NLL requirements in both active and reactive power. before the load variation ([t = 0s to t = 1s]), the maximum extracted PV power fed by the APF is more than that drawn by the connected NLL , the extra part of power after fulfilling the load demand is fed to the utility grid, this is characterized by a negative sign of the grid power (Figure 11) and the opposition in phase between grid current and voltage (Figure 12(a)), After the load variation [t=1s to t= 2s], the load required power is greater than that injected by the APF from the PVS, to fulfill the load demand, the grid compensates the deficit of power and shares the load power with the PVS, This is characterized by a positive sign of the grid power (Figure 11) and the grid voltage in phase with the grid current (Figure 12(b)).

5.2 Mode of operation 2 (APF mode)

This mode of operation is functional when the PVS is non-operational, there is no power injected from the GPV for any reasons. In this case; the NLL required active power is totally supplied by the grid (Figure 13) which explain the synchronization and the increase in the amplitude of the grid

currents (Figure 14), In this mode, the TTLNPC based APF ensure only the NLL requirements in terms of reactive power and harmonic currents, these results can be shown clearly in the Figure 14 where the grid currents still have its sinusoidal form with a good quality and a very-good reduction of harmonics.

It can be seen from the Figure 15 that the reactive power of the load is equal to that fed by the TTLNPC inverter based APF in the two operation modes. This proves the succeed of the APF to feed the needed reactive power independently of the extracted PV power (Figure 15).

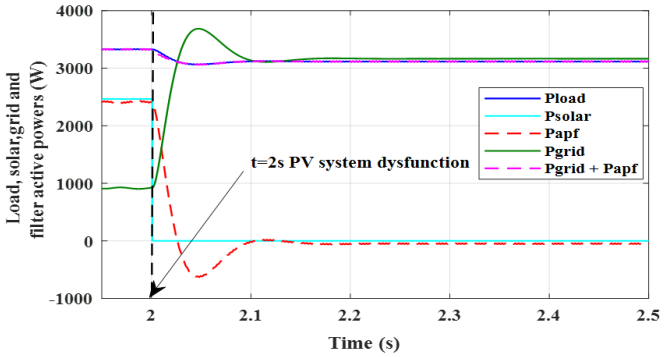

Figure 13. Load power sharing after PVS dysfunction

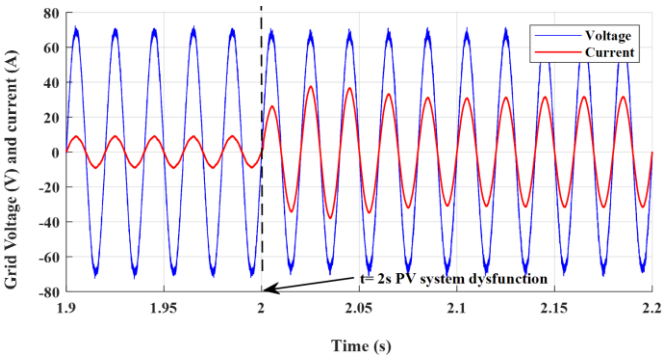

Figure 14. Grid voltage and current when the PVS is non-operational

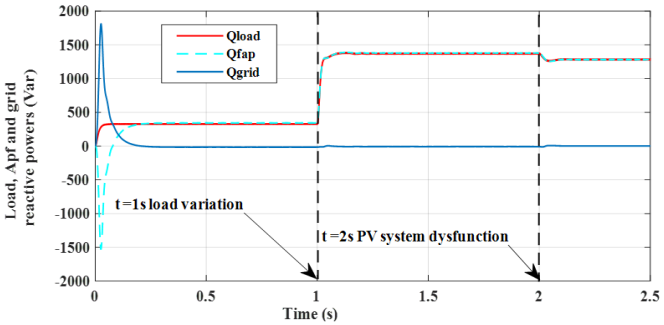

Figure 15. Look of the load, grid and APF reactive power

Figure 16 shows the waveforms and the harmonic contenent of the grid current in the two operational modes with $\lambda_c = 0.5$, $\lambda_{sw} = 0$ (in opposite and in phase with the grid voltage). Without taking into consideration the reduction of SWF, the results prove that the FCS-MPC applied to the TTLNPC inverter based APF gives good performance to predict the APF compensation current in dynamic response (fast tracking) and steady state (high stability) compared to the predictive control applied to the 2L three-phase inverter proposed by the authors [22, 25]. The FCS-MPC has demonstrated its effectiveness to estimate the filter reference currents with the minimum possible error due to the selection of the optimal SS corresponding the optimal voltage vector at every sample time T_s, this interprets the improved form (sinusoidal shape) of the grid current and the values of THDi = 0.57% and 0.86% in the two mentioned cases.

The results in Figure 17 show that the reference, predicted and measured filter currents are superimposed, this result proves the effectiveness of the FCS-MPC in dynamic and steady states to predict the filter currents at each sampling time T_s. Also, Figures 18 and 19 prove the success of the FCS-MPC in predicting and maintaining the whole dc-link voltages (V_c, V_{c1} and V_{c2}) of the TTLNPC inverter based APF (in the two operation modes) controlled at their reference values. Moreover, the FCS-MPC succeeded in maintaining a voltage balance across both of two capacitor voltages (V_{c1} and V_{c2}) and each is as half of the overall dc-link voltage V_c. these findings show also the effectiveness of the selected cost function applied to achieve the balance of the neutral point voltages.

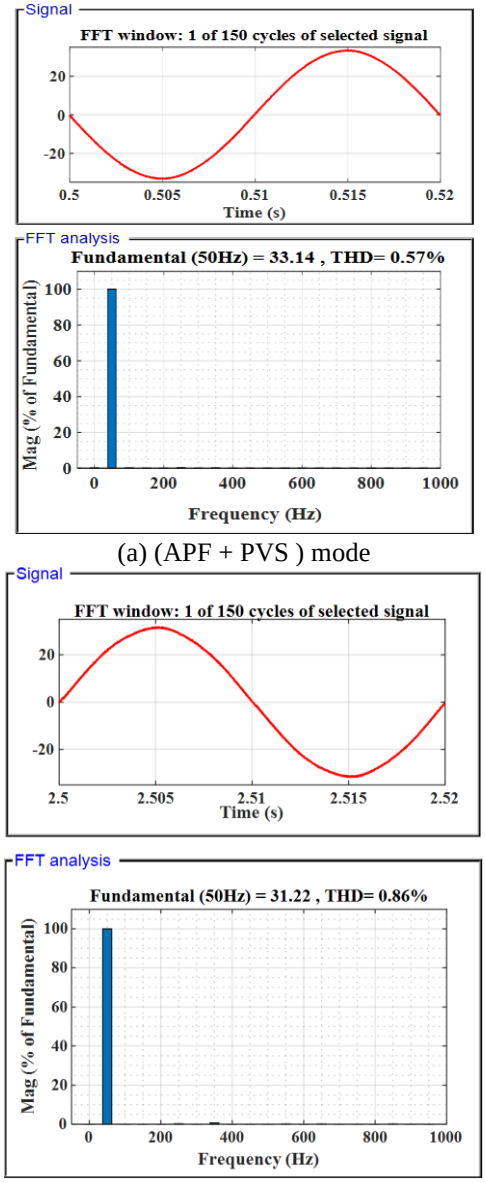

(a) (APF + PVS) mode

(b) APF mode

Figure 16. Waveform and harmonic continent of grid current with $\lambda_c = 0.5$, $\lambda_{sw} = 0$

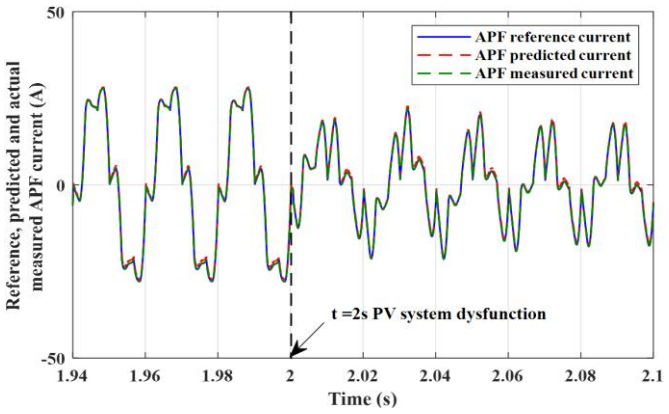

Figure 17. Reference, predicted and measured filter currents

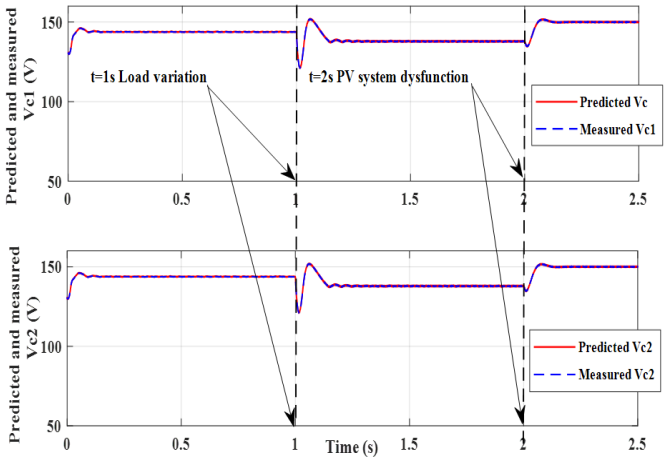

Figure 18. Predicted and measured capacitor voltages V_{c1} and V_{c2}

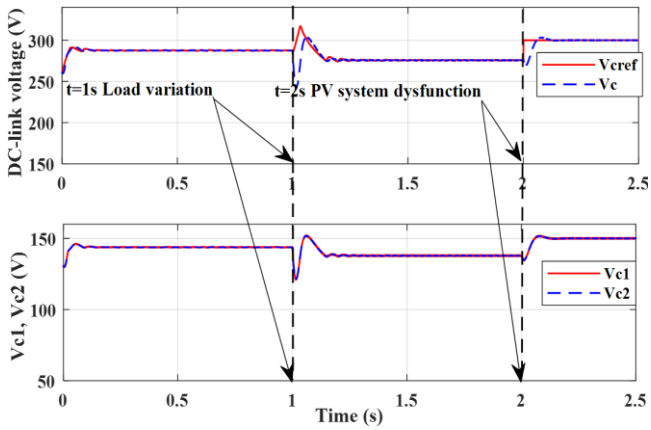

Figure 19. Look of the measured dc-link voltages after control

5.3 Effect of SWF reduction

In this section, the SWF reduction will be taken into account. Higher the value of λ_{sw}, higher the reduction of SWF and consequently the switching losses. The Figure 20 (a and b) shows the effect of increasing λ_{sw} to 0.5 and 1 respectively, it can be seen that the switching losses has been attenuated; this interpreted by the increase of the injected grid current fundamental component amplitude from ($i_{g,f} = 33.14A$, $\lambda_{sw} = 0$) to ($i_{g,f} = 34.06A$, $\lambda_{sw} = 1$) (close to 1A has been compensated) when the PVS is operational (Mode 1). In mode 2 where the PVS is non-operational, increasing the value of λ_{sw} decrease the drawn grid current fundamental component amplitude from ($i_{g,f} = 31.22A$, $\lambda_{sw} = 0$) to ($i_{g,f} = 30.62A$,$\lambda_{sw} = 1$). about 0.6A has been compensated which light the burden on the grid utility.

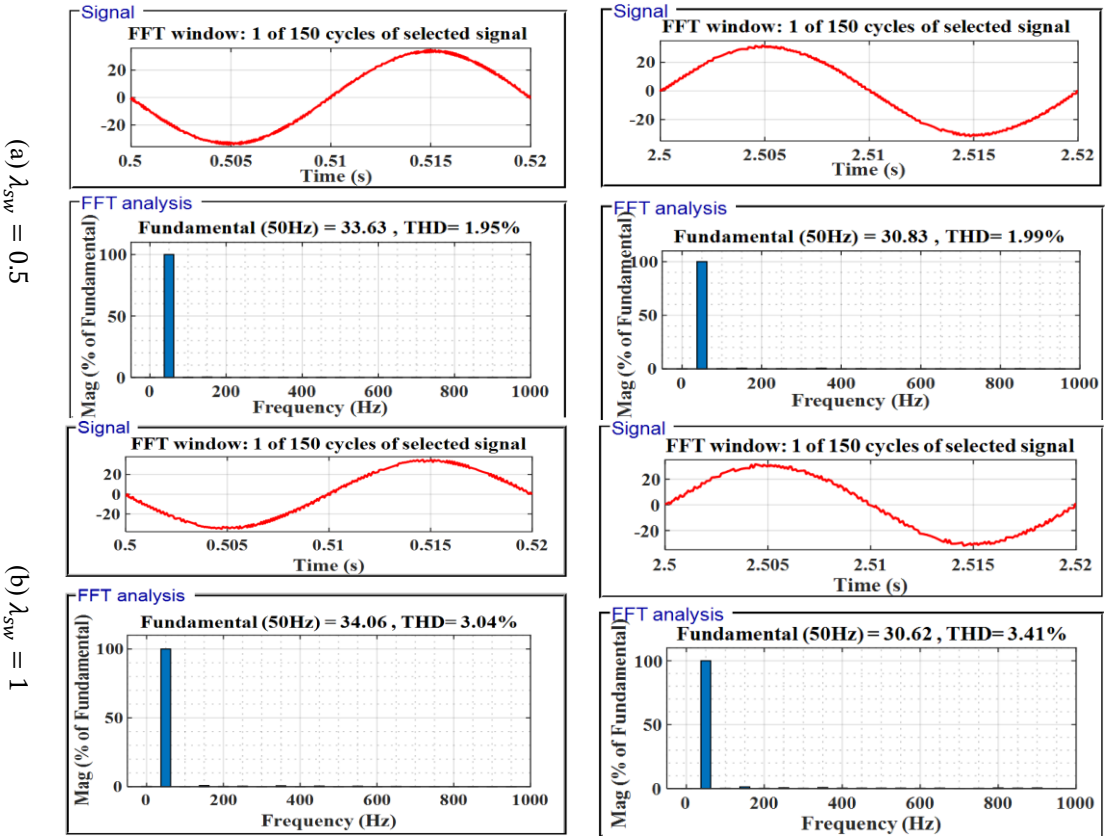

Figure 20. Effect of the SWF reduction on the power quality improvement

On the other hand, increasing the value of λ_{sw} affect the power quality of the power fed to the PCC via the TTLNPC inverter based APF. The grid current waveforms and the increased values of THDi prove that the performance of the FCS-MPC to track the APF reference current has been reduced. Hence, the value of λ_{sw} should be selected properly to fit the control requirement in terms of reference tracking and SWF.

6. CONCLUSION

In this paper, the control of TTLNPC inverter based APF interfacing a PVS to the grid has been achieved using the finite control set model predictive control. the principle of the FCS-MPC is simple, does not require any kind of modulator or linear controller. These advantages make it easy to understand and implement. The simulation finding results show the robustness and the effectiveness of the predictive control proposed for the NPC inverter to estimate the filter reference currents under variable changing in the climatic conditions (solar irradiance) as well as changing operating modes (APF+PV, APF only) which is clearly shown in the best found values of the grid current THDi compared to those obtained by the predictive control applied to the most popular 2L inverter [22, 25].

With a proper value of λ_{sw} and λ_c, The TTLNPC inverter based APF has proven its effectiveness as a good solution to interface and feed the maximum available PV to the power grid and share with it the load power demand. This novel PVS interfacing three-phase TTLNPC based APF has been proposed to light the burden on the power grid by reducing the power drawn from it and preserving the sinusoidal shape of its current. Any extra amount of power after fulfilling the load power is fed to the grid.

It's worthy to note that the reactive power has been compensated, the grid current waveforms has been improved, the load power sharing has been performed, which means that the two functions assigned to the filter has been accomplished.

REFERENCES

[1] Teodorescu, R., liserre, M., rodriguez, P. (2011). Grid converters for photovoltaic and wind power systems. John Wiley & Sons. https://doi.org/10.1002/9780470667057

[2] Deutsche Gesellschaft für Sonnenenergie (DGS). (2013). Planning and installing photovoltaic systems: A guide for installers, architects and engineers. Routledge.

[3] Wang, F., Duarte, J.L., Hendrix, M.A. (2011). Grid-interfacing converter systems with enhanced voltage quality for microgrid application-Concept and implementation. IEEE Transactions on Power Electronics, 26(12): 3501-3513. https://doi.org/10.1109/TPEL.2011.2147334

[4] Sezen, S., Aktas, A., Ucar, M., Ozdemir, E. (2014). A three-phase TTLNPC inverter based grid-connected photovoltaic system with active power filtering. In 2014 16th International Power Electronics and Motion Control Conference and Exposition, Antalya, Turkey, pp. 1331-1335. https://doi.org/10.1109/EPEPEMC.2014.6980697

[5] Yang, B., Li, W., Zhao, Y., He, X. (2009). Design and analysis of a grid-connected photovoltaic power system. IEEE Transactions on Power Electronics, 25(4): 992-1000. https://doi.org/10.1109/TPEL.2009.2036432

[6] Wu, T.F., Chang, C.H., Lin, L.C., Kuo, C.L. (2011). Power loss comparison of single-and two-stage grid-connected photovoltaic systems. IEEE Transactions on Energy Conversion. 26(2): 707-715. https://doi.org/10.1109/TEC.2011.2123897

[7] Kouro, S., Leon, J.I., Vinnikov, D., Franquelo, L.G. (2015). Grid-connected photovoltaic systems: An overview of recent research and emerging PV converter technology. IEEE Industrial Electronics Magazine, 9(1): 47-61. https://doi.org/10.1109/MIE.2014.2376976

[8] Satti, M.B., Hasan, A., Ahmad, M.I. (2018). Direct model predictive control of novel H-bridge multilevel inverter based grid-connected photovoltaic system. IEEE Access, 7: 62750-62758. https://doi.org/10.1109/ACCESS.2019.2916195

[9] Kalra, K.P.K., Shah, M.T. (2017). Simulation analysis of two-level and three-level (NPC) converter based SAPF for different current control schemes. In 2017 Recent Developments in Control, Automation & Power Engineering (RDCAPE), Noida, India, pp. 212-219. IEEE. https://doi.org/10.1109/RDCAPE.2017.8358269

[10] Hoon, Y., Radzi, M.A.M., Hassan, M.K., et al. (2016). A simplified synchronous reference frame for indirect current controlled three-level inverter-based shunt active power filters. Journal of Power Electronics, 16(5): 1964-1980. https://doi.org/10.6113/JPE.2016.16.5.1964

[11] Hoon, Y., Radzi, M.A.M., Hassan, M.K., Mailah, N.F. (2017). Operation of three-level inverter-based shunt active power filter under non-ideal grid voltage conditions with dual fundamental component extraction. IEEE Transactions on Power Electronics, 33(9): 7558-7570. https://doi.org/10.1109/TPEL.2017.2766268

[12] Alonso-Mart, J., Arnaltes, S. (2010). Direct power control of grid connected PV systems with three level NPC inverter. Solar Energy, 84(7): 1175-1186. https://doi.org/10.1016/j.solener.2010.03.023

[13] Colak, I., Kabalci, E., Bayindir, R. (2011) Review of multilevel voltage source inverter topologies and control schemes. Energy Conversion and Management, 52(2): 1114-1128. https://doi.org/10.1016/j.enconman.2010.09.006

[14] Boukezata, B., Chaoui, A., Gaubert, J.P., Hachemi, M. (2014). Système solaire photovoltaïque connecté au réseau électrique et associé à un filtre actif parallèle. Symposium de Génie Électrique, Cachan, France. hal-01065188

[15] Khadkikar, V., Chandra, A., Singh, B.N. (2009). Generalized single-phase PQ theory for active power filtering: simulation and DSP-based experimental investigation. IET Power Electronics, 2(1): 67-78. https://doi.org/0.1049/iet-pel:20070375

[16] Ochoa-Giménez, M., Roldán-Peréz, J., Garcia-Cerrada, A., Zamora-Macho, J.L. (2015). Efficient multiple-reference-frame controller for harmonic suppression in custom power devices. International Journal of Electrical Power & Energy Systems, 69: 344-353. https://doi.org/10.1016/j.ijepes.2015.01.013

[17] Sundaram, E., Venugopal, M. (2016). On design and implementation of three phase three level shunt active power filter for harmonic reduction using synchronous reference frame theory. International Journal of Electrical Power & Energy Systems, 81: 40-47. https://doi.org/10.1016/j.ijepes.2016.02.008

[18] Chaoui, A., Gaubert, J., Bouafia, A. (2013). Direct power control switching table concept and analysis for three-phase shunt active power filter. Journal of Electrical Systems, 9(1): 52-65. https://doi.org/10.1109/IECON.2012.6388553

[19] Djazia, K., Krim, F., Chaoui, A., Sarra, M. (2015). Active power filtering using the ZDPC method under unbalanced and distorted grid voltage conditions. Energies, 8(3): 1584-1605. https://doi.org/10.3390/en8031584

[20] Gherouat, O., Hassam, A., Aissa, O., Babes, B. (2021). Experimental evaluation of single-phase shunt active power filter based on optimized synergetic control strategy for power quality enhancement. Journal Eropéen des Systèmes Automatisés, 54(4): 649-659. https://doi.org/10.18280/jesa.540415

[21] Chilipi, R., Al Sayari, N., Al Hosani, K., et al. (2018). Third order sinusoidal integrator (TOSSI)-based control algorithm for shunt active power filter under distorted and unbalanced voltage conditions. International Journal of Electrical Power & Energy Systems, 96: 152-162. https://doi.org/10.1016/j.ijepes.2017.09.026

[22] Lakhdari, A., Krim, F., Borni, A. (2019). Model predictive control for an APF interfaced by a wind energy conversion system. Journal of Engineering Research, 7(1): 3840.

[23] Kouro, S., Cortés, P., Vargas, R., et al. (2008). Model predictive control - A simple and powerful method to control power converters. IEEE Transactions on Industrial Electronics, 56(6): 1826-1838. https://doi.org/10.1109/TIE.2008.2008349

[24] Tarisciotti, L., Formentini, A., Gaeta, A., et al. (2016). Model predictive control for shunt active filters with fixed switching frequency. IEEE Transactions on Industry Applications, 53(1): 296-304. https://doi.org/10.1109/TIA.2016.2606364

[25] Boukezata, B., Gaubert, J.P., Chaoui, A., Hachemi, M. (2016). Predictive current control in multifunctional grid connected inverter interfaced by PV system. Solar Energy, 139: 130-141. https://doi.org/10.1016/j.solener.2016.09.029

[26] Rodriguez, J., Cortes, P. (2012). Predictive Control of Power Converters and Electrical Drives. John Wiley & Sons.

[27] Vargas, R., Cortés, P., Ammann, U., et al. (2007). Predictive control of a three-phase neutral-point-clamped inverter. IEEE Transactions on Industrial Electronics, 54(5): 2697-2705. https://doi.org/10.1109/TIE.2007.899854

[28] Rodriguez, J., Pontt, J., Silva, C.A., Correa, P., Lezana, P., Cortes, P., Ammann, A. (2007). Predictive current control of a voltage source inverter. IEEE Transactions on Industrial Electronics, 54(1): 495-503. https://doi.org/10.1109/TIE.2006.888802